Fracture simulation of concrete beams to assess softening behavior by varying different fractions of aggregates

H. S. Vishwanatha, S. Muralidhara
B.M.S. College of Engineering, Department of Civil Engineering, Vishveshwarya Technical University, Bangalore, Karnataka, India
vishwanathahs@bmsce.ac.in, murali.civ@bmsce.ac.in

B. K. Raghu Prasad
Department of Civil Engineering, Indian Institute of Science, Bangalore, Karnataka, India
bkriisc@gmail.com

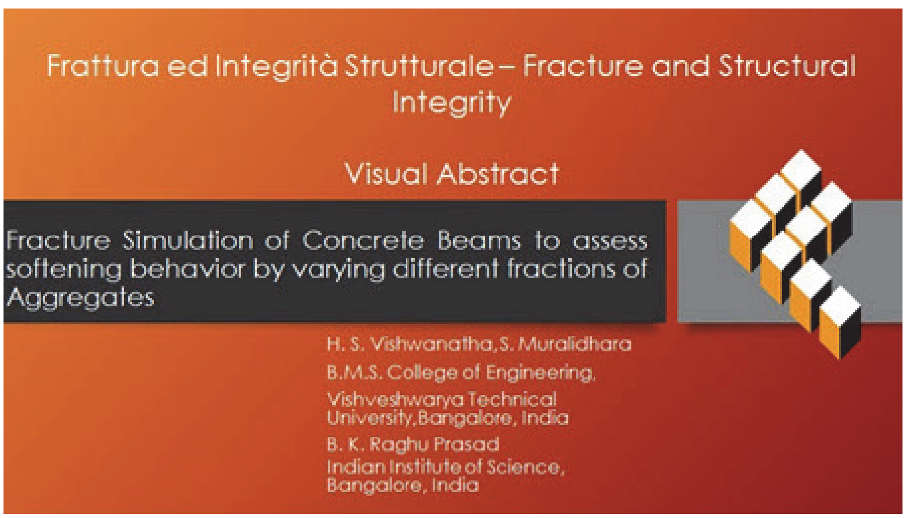

OPEN ACCESS

Citation: Vishwanatha, H., Murlidhara, S., Raghu Prasad, B. Fracture Simulation of Concrete Beams to assess softening behavior by varying different fractions of aggregates, Frattura ed Integrità Strutturale, 67 (2024) 43-57.

Received: 02.09.2023
Accepted: 21.10.2023
Online first: 28.10.2023
Published: 01.01.2024

KEYWORDS. Coarse aggregate, Randomness, Fracture energy, Load-deflection, Interfacial Transition Zone.

INTRODUCTION

Concrete undergoes various adverse loading conditions. During seismic loads, ductility plays an important factor [40]. Most of the concrete structures were designed considering bending moments and shear forces. Concrete, with its heterogeneous mesostructure, demonstrates complex mechanical responses when subjected to high-rate loads [29]. A comprehensive description of failure mechanisms is crucial to ensuring the safety of concrete structures [27]. During the design, importance is not emphasized on concrete behavior during fracture, which is significantly important during the post-peak softening process [6].
Several computational techniques have been utilized to simulate concrete materials. Many of these models primarily focused on homogenized macroscopic material behavior, often neglecting the intricate micro- or meso-structure of concrete materials [3, 15, 17]. Concrete comprises three phases: the mortar, the coarse aggregates, and the interfacial transition zone (ITZ) situated between the aggregate and mortar [9, 10, 28].

Simulating the post-peak softening process using mesostructures of concrete consisting of a three-phase system is a challenging job [33]. The latest studies show that computed tomography scans can be used to generate the mesostructures of concrete, which involves complexity and high cost [19, 24]. To achieve a realistic simulation within a reasonable computation time, finite element analysis yields favorable results [26]. The cracking behavior in numerical simulations can be modeled using the softening (failure) behavior of concrete [5, 8, 18, 7].
The surface-based cohesive zone model between the aggregate and cement matrix was simulated using the Traction Separation Law (TSL) [41]. The fundamental concept of the cohesive zone model, initially proposed by Barenblat [1], is to investigate the behavior of the material within a region directly ahead of a traction-free crack tip. Hillerborg introduced the initial cohesive crack model to simulate discrete cracks in the fracture process zone (FPZ) of concrete [2]. The cohesive zone model is a straightforward approach to modeling the fracture of concrete specimens, demonstrating strong agreement with experimental results. It can effectively predict the behavior of intact structures [11]. Crack propagation can be simulated using the XFEM method, in which material properties can be provided as input under damage for TSL initiation [12, 20, 30]. Both the relative proportion of aggregates and the ITZ assume pivotal roles in determining the behavior of concrete grades during the fracture process.
The present study consists of creating finite element models of different fractions of aggregate and cement matrix along with ITZ and studying the post-peak softening behavior of concrete models. The models were validated using experimental data.
The study focuses on analyzing various aggregate fractions and investigating the influence of the Interfacial Transition Zone (ITZ) during the fracture process. The final conclusion is drawn from the analysis of load-deflection curves obtained from simulations.

NUMERICAL SIMULATIONS

The present work involves the numerical modeling of fracture tests of geometrically similar three-point bending (TPB) beams with a constant length-to-depth ratio. The simulation of the TPB specimen performed by the finite element analysis incorporating the concrete softening behavior predicts the load-displacement curves.

Length (mm)	Effective Span (l) (mm)	Width (mm)	Depth (mm)	Notch-to-depth ratio	Initial notch depth (mm)
375	282	47.5	95	0.25	23.75

Table 1: Geometrical properties of the beam (SB-1).

The 2D beam models were developed using a Python script to study the effects of different proportions of coarse aggregates (uniform size and distributed size) and cement matrix, both with and without an Interfacial Transition Zone (ITZ). The boundary conditions were applied to simulate simply supported conditions.
The loading was applied in a displacement-controlled manner by means of an analytically rigid body acting on the upper surface of the beam in its mid-span. The loading allows for crack penetration through the entire beam height. Adequate contact properties between supports and beams are applied.
In essence, crack propagation and fracture in concrete numerical simulations are intricately tied to mesh generation. Recognizing the influence of mesh sizes on numerical simulations, the present study investigated five distinct mesh sizes (0.5mm, 0.75mm, 1mm, 2mm, and 4mm) [36]. Notably, mesh sizes less than 1mm in the current study's model result in the development of inadequately meshed regions for fine meshes and element distortion with unfavorable mesh angles for coarser meshes. Since a 1mm mesh size was used in many studies [25, 29, 27], the different mesh sizes were set around 1 mm in this study. A concrete beam is modeled by solid, deformable, finite elements meshed with quad elements. XFEM parameters are provided using the Abaqus-Cae software.

GENERATION OF RANDOM AGGREGATES

The mortar, which is made of fine aggregates and cement, usually serves as the composite matrix. The aggregates, being the strongest component, make up about 75% of the concrete volume, with 40–50% of them being coarse aggregates depending on different design mixes. The ITZ, typically forming around the aggregates, is generally regarded as the weakest part [17, 28, 39]. For the present study, covering a range from low-strength concrete (M20) to high-strength concrete (up to M45), aggregate fractions of 38%, 40%, 50%, and 54% were selected [32]. Spherical aggregates were randomly distributed and used in this study.

The aggregates are generated with a random distribution within the specified size of the model and the aggregate fraction by adopting the Monte Carlo method [16]. Aggregates are placed without overlapping each other. To ensure this condition is met, a loop to check and reject functions has been coded in the Python script. During the distribution process, small gaps are specifically created for the cement matrix. The number of iterations should be defined before running the script.

The Python code was developed to generate concrete mesostructures with aggregate volume fractions of up to 54%. But when dealing with instances where the aggregate volume fraction exceeds 54%, the computational demands notably increase. This increase leads to a greater demand for conducting intersection checks among aggregate particles that are already positioned, along with a decreased probability of identifying empty spaces within the mortar matrix. The Python script is designed for creating models, positioning aggregates, defining and assigning material properties, creating steps, loading and assigning boundary conditions, assembling and developing interactions with the model, and meshing complete, which can be directly submitted for job-run analysis. The aggregate positions are changed by each iteration in the Python script. For the present study, three iterations are considered for each case (Model-1, Model-2, and Model-3).

GENERATION OF RANDOM AGGREGATES COHESIVE ELEMENT MODEL OF THE INTERFACIAL TRANSITION ZONE (ITZ)

The thickness of the ITZ lies between 10 and 50 μm; achieving this level of precision using the Finite Element Method (FEM) proves challenging. As a solution, the present work employs the Cohesive Element Model (CEM) to simulate the ITZ [41]. In this context, the ITZ is treated as having a thickness of zero [38], which retains the relevant mechanical properties of the actual ITZ to achieve the accuracy of the simulation, and all ITZs in concrete can be represented by a zero-thickness element.

This can be achieved by the following methods:

i) Cohesive elements share nodes with other elements.

ii) Contact interactions between cohesive elements and other features.

iii) Contact interaction with the cohesive zone and one part.

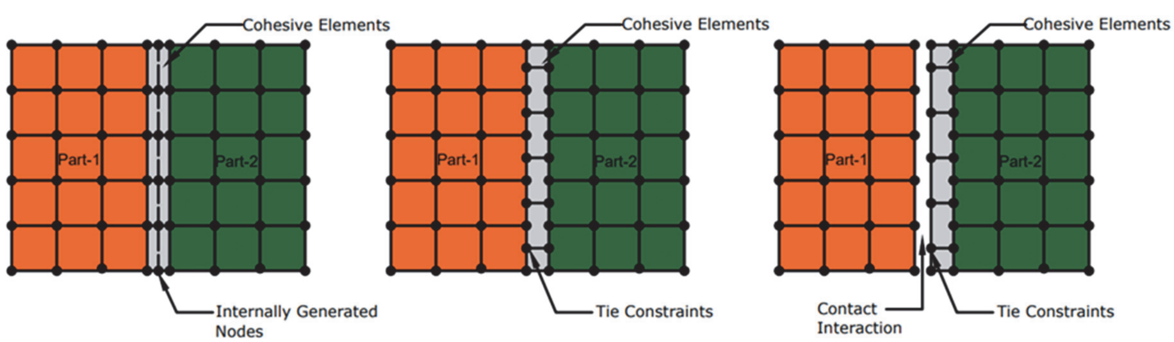

a. Shared nodes b. Contact interaction with both parts c. Contact interaction with one part

Figure 1: Cohesive Element Models

The first approach adopted in the present study is to create a zero-thickness cohesive zone on the contact surface of the aggregate and mortar. ITZ properties are assigned to the cohesive zone using a Python script in the finite element software [34].

The deterioration of the Cohesive Element (CE) is categorized into four distinct phases: the initial linear elastic phase, the phase of damage initiation, the phase of damage progression, and the ultimate complete damage phase. The phase that pertains to the CE's ability to sustain damage while still maintaining its functionality is referred to as the online resilience phase of the CE's damage response.

In the present study, the cohesive zone model is adopted to simulate fracture in a particular zone. However, it does not yield any damage fracture since we are adopting the XFEM method.

FINITE ELEMENT MODELS

The proposed finite element models for the present study are shown in Fig. 2. The material properties considered for analysis [30]:

Element	E (GPa)	υ	σ_0	G (N/m)
Aggregate	50	0.16		
Mortar	24.7	0.20	3.17	168
ITZ	21.2	0.20	2.4	115

Table 2: Material Properties

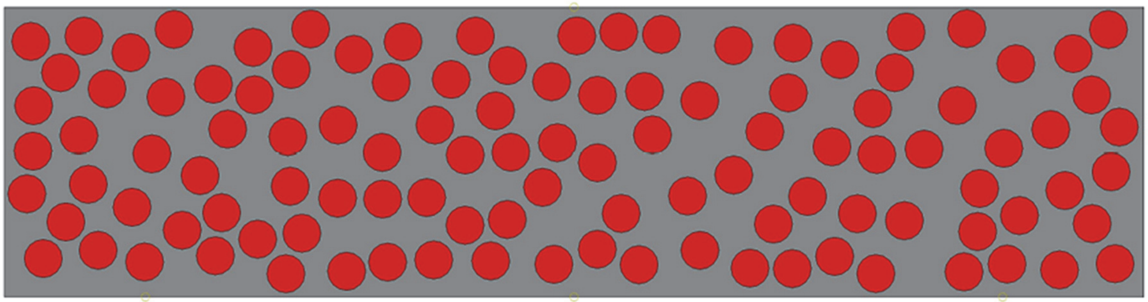

I. CA of 12.5mm mean size and cement matrix (CA-Matrix -Case1(a))

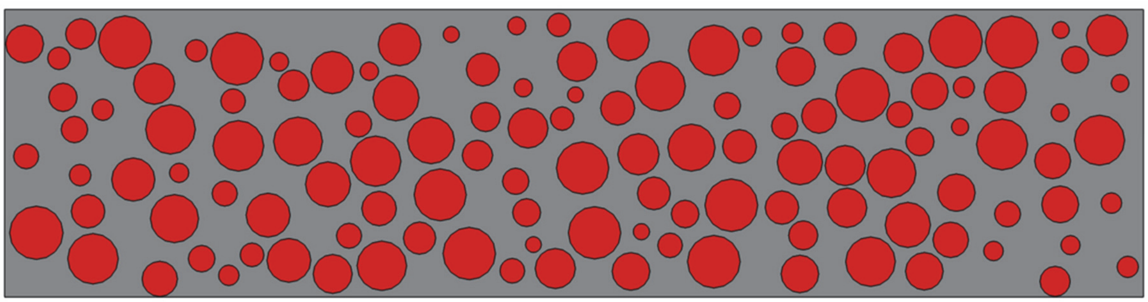

II. CA of 4.75 mm to 20mm size and cement matrix (CA-Matrix -Case1(b))

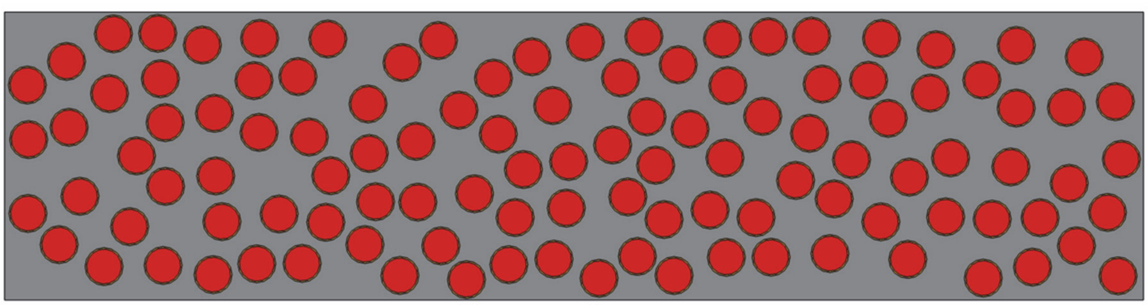

III. CA of 12.5mm mean size and cement matrix along with ITZ (CA-Matrix-ITZ -Case2(a)).

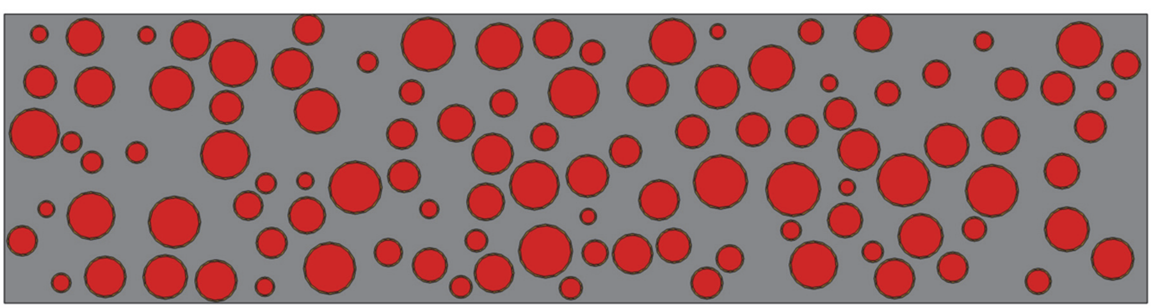

IV. CA of 4.75 mm to 20mm size and cement matrix along with ITZ (CA-Matrix-ITZ -Case2(b))

Figure 2: Finite-element grid model of concrete three-point bending beam with and without ITZ for 38% fraction of CA

Validation of Numerical Modeling Method

After adjusting the input parameters of the TSL based on calibration, we carried out mesoscale concrete simulations [41]. These simulations were then validated against experimental results obtained from TBD fracture tests in reference [39]. To the validate model, three different FE models of length = 400 mm, breadth = 100 mm, and depth = 100 mm with notch depth = 25 mm were developed using a Python script, each with varying aggregate distributions, covering a volume fraction range of 38% to 54%. The model's reliability was checked by the normal distribution and the Gaussian probability density function. The XFEM method is adopted for simulations. The load-deflection curves were plotted by averaging the results from each of these simulations. Fig. 3 shows the load-deflection curves plotted from the TBD simulations, along with the experimental data.

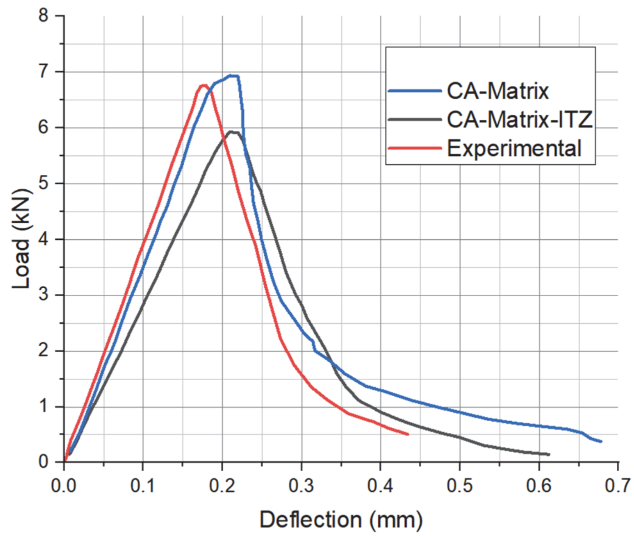

Figure 3: Comparison between experimental and numerical load–displacement curves.

Comparing the numerical simulations with the experimental results yielded remarkable consistency, affirming the capability of the proposed approach to accurately predict crack initiation and propagation in composite materials like concrete. The average peak load values recorded during the experiments were 6.54 kN, while the result obtained from the simulation was 5.95 kN. This slight deviation of approximately 10% lower results in the simulations compared to the experimental study can be attributed to the simplifications made in the analysis, such as the use of circular aggregates and the adoption of a two-dimensional plane stress model. These simplifications were necessary to manage computational time and memory consumption, as a full 3-D analysis would have been significantly more resource-intensive. Furthermore, when examining the post-peak softening slope (represented by tan θ), the experimental study yielded an average value of 51, whereas the result from the simulation yielded 41.67. This range in the simulation results closely aligns with the observed real-world behavior, suggesting that our FE model analysis produced a realistic curve reflecting the concrete's response during and after the peak load

Results and discussion

As expected, crack initiation occurred at the pre-existing notch located at the midpoint of the beam and propagated towards the loading point [7]. This cracking progression traversed through the Interfacial Transition Zone (ITZ) and the cement paste phases, both of which are weaker materials while attempting to bypass the aggregates, as depicted in Fig. 5.b.This observed crack development is reasonable, as aggregates are inherently stronger than the other two phases. Furthermore, it is noteworthy that this crack pattern closely resembles the cracks observed in Kozicki's model [13], which serves to validate our current model.

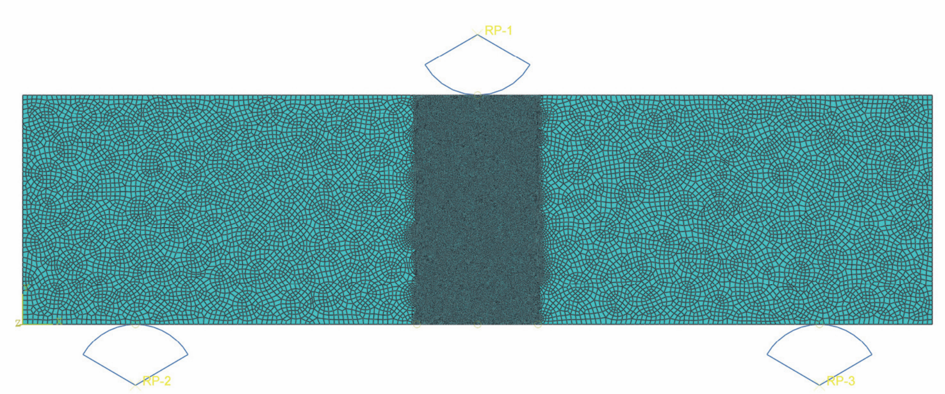

a. Meshed beam under load

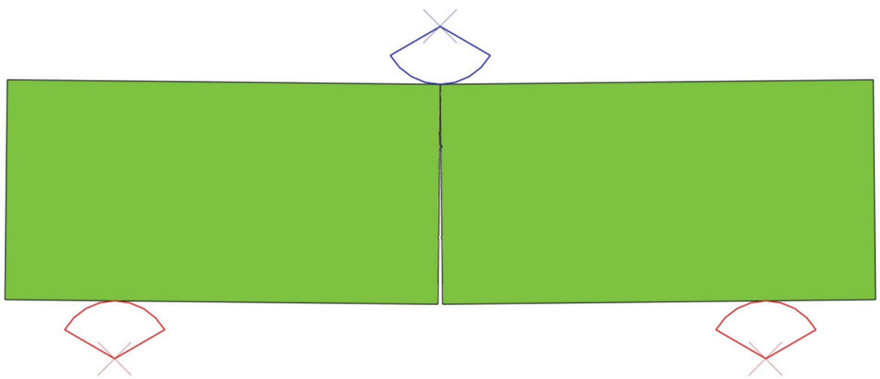

b. Deflected beam under peak load

Figure 4: Crack propagation in CA-Matrix.

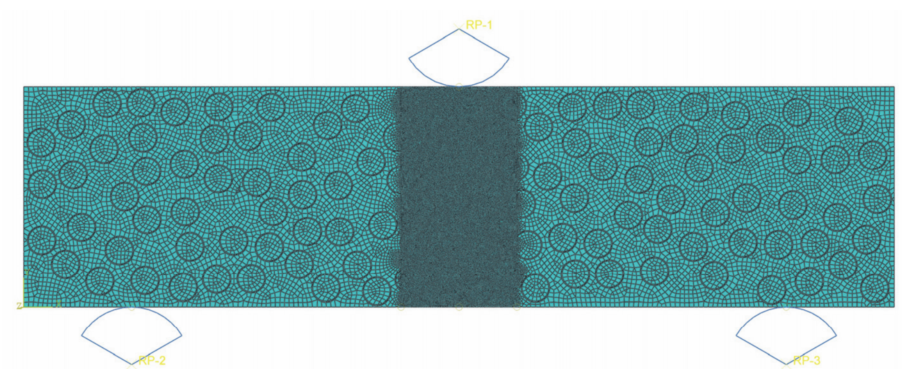

a. Meshed beam under load

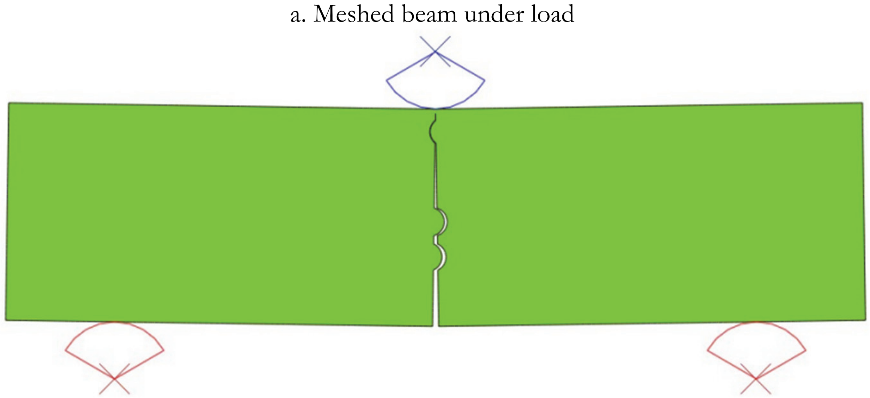

b. Deflected beam under peak load

Figure 5: Crack propagation in CA -Matrix -ITZ.

Fraction of CA		Mean size of Aggregate12.5mm (a) 54%	50%	40%	38%	Aggregate size between 4.75mm to 20mm (b) 54%	50%	40%	38%
S-B1	Model-1	2.8	3.2	5	3.9	5	4.5	5	4.8
	Model-2	2.9	3.5	4.7	3.8	4.8	4	5.2	5
	Model-3	3.2	3.1	4.2	4.0	4.7	4.3	5.3	5.1
Mean (μ)		2.97	3.27	4.63	3.90	4.83	4.27	5.17	4.97
Standard Deviation (σ)		0.17	0.17	0.33	0.08	0.12	0.21	0.12	0.12
μ±3σ (99.7%)		3.48	3.78	5.62	4.14	5.21	4.88	5.54	5.34
		2.46	2.76	3.64	3.66	4.46	3.65	4.79	4.59

Table 3: Ultimate load (kN) for Case1(a) and (b)

Fraction of CA		Mean size of Aggregate12.5mm (a) 54%	50%	40%	38%	Aggregate size between 4.75mm to 20mm (b) 54%	50%	40%	38%
S-B1	Model-1	2.5	2.7	3.4	3.5	2.2	2.8	3.2	3.5
	Model-2	2.6	2.8	3.2	3.2	2.7	2.9	3.1	3.4
	Model-3	2.1	2.7	3.3	3.7	2.5	2.5	3.3	3.6
Mean (μ)		2.40	2.73	3.30	3.47	2.47	2.73	3.20	3.50
Standard Deviation(σ)		0.22	0.05	0.08	0.21	0.21	0.17	0.08	0.08
μ±3σ(99.7%)		3.05	2.87	3.54	4.08	3.08	3.24	3.44	3.74
		1.75	2.59	3.06	2.85	1.85	2.22	2.96	3.26

Table 4: Ultimate load (kN) for Case2(a) and (b)

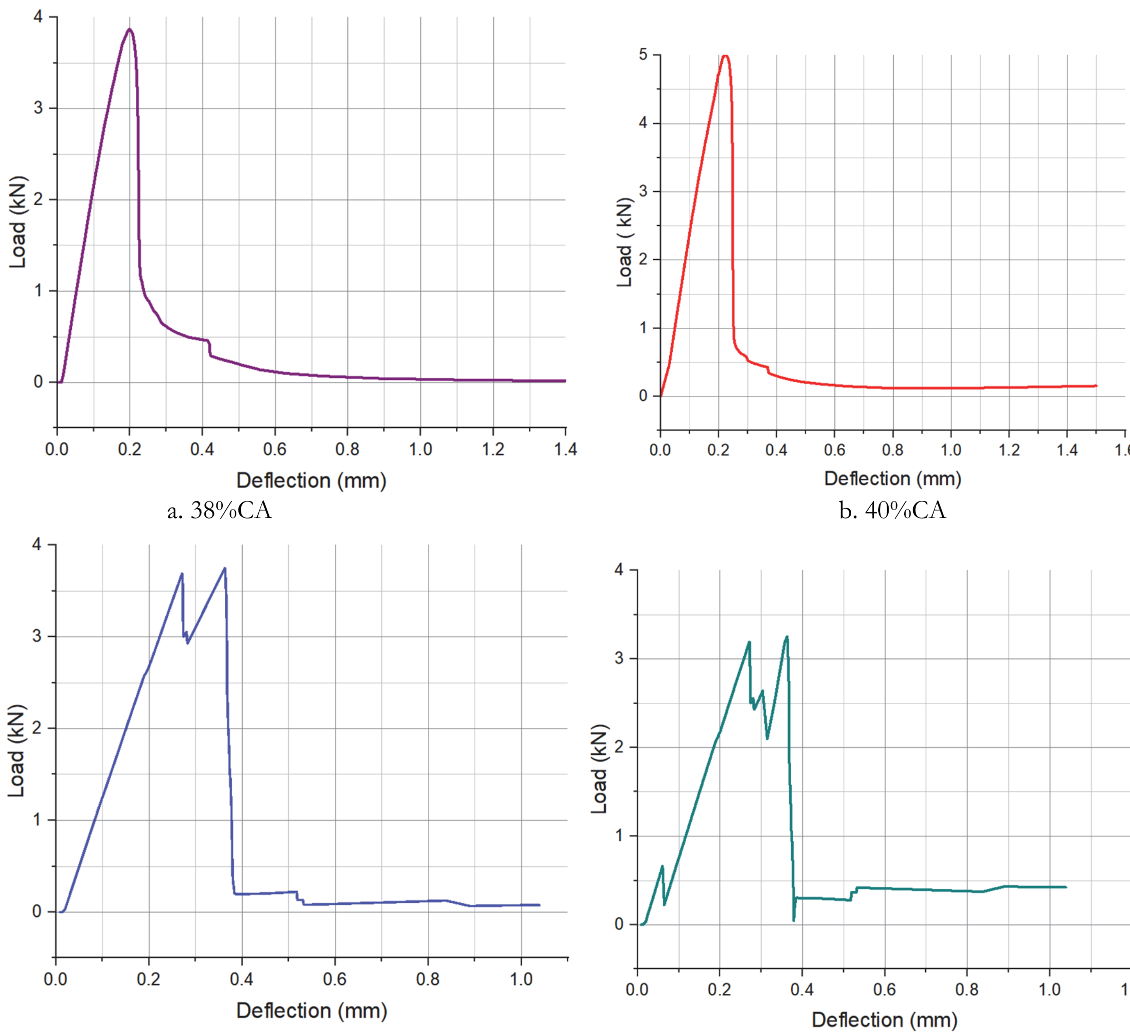

a. 38%CA b. 40%CA

c. 50%CA d. 54%CA

Figure 6: Case1(a) Load -Deflection curve for CA of mean size 12.5mm.

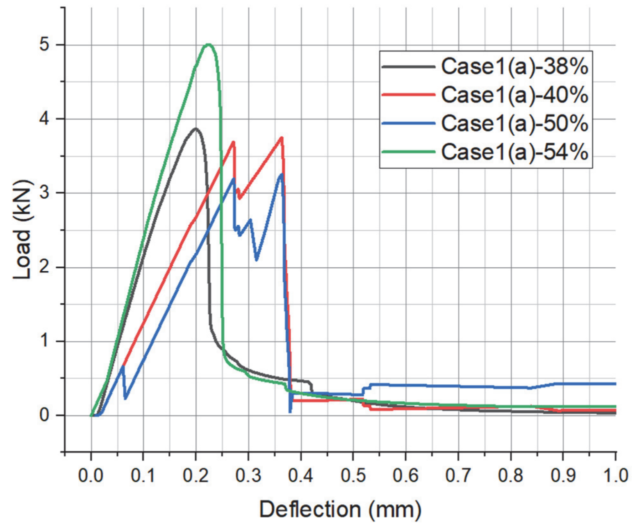

Figure 7: Case1(a) Load-Deflection comparison.

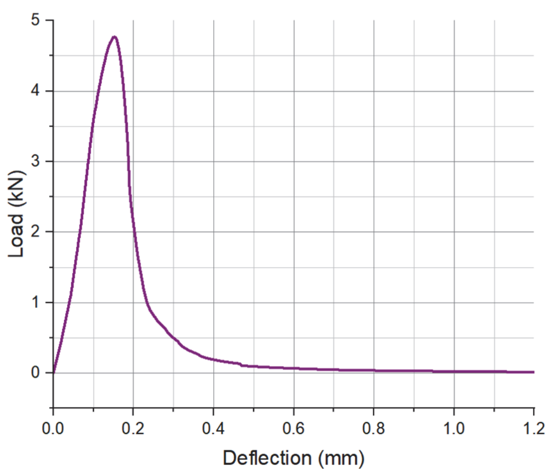

a. 38%CA

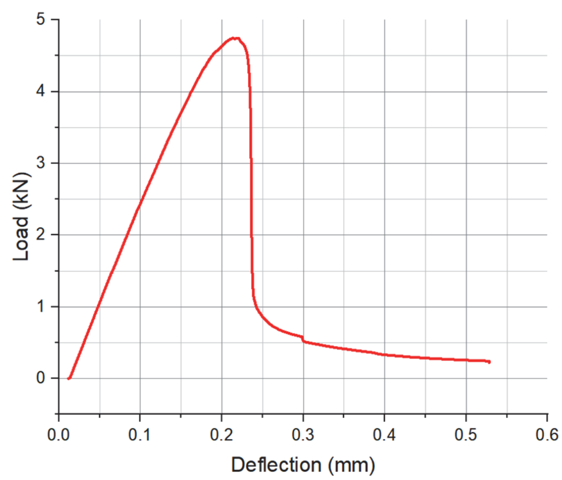

b. 40%CA

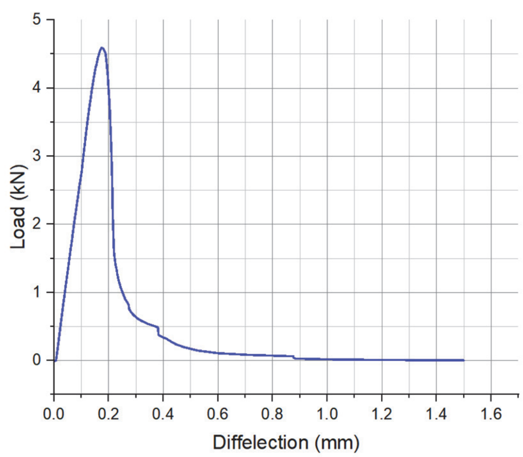

c. 50%CA

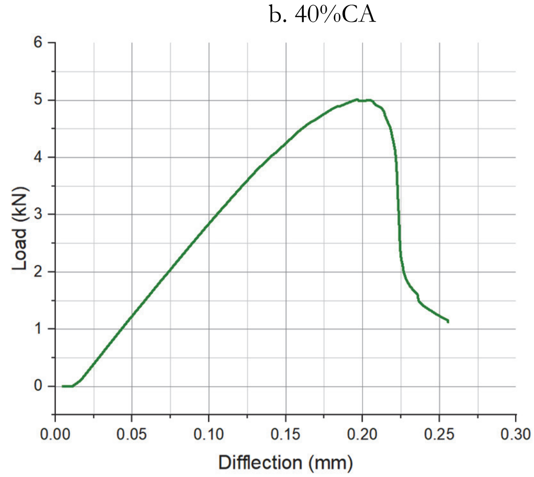

d. 54%CA

Figure 8: Case1(b) Load -Deflection curve for CA of size between 4.75mm to 20mm.

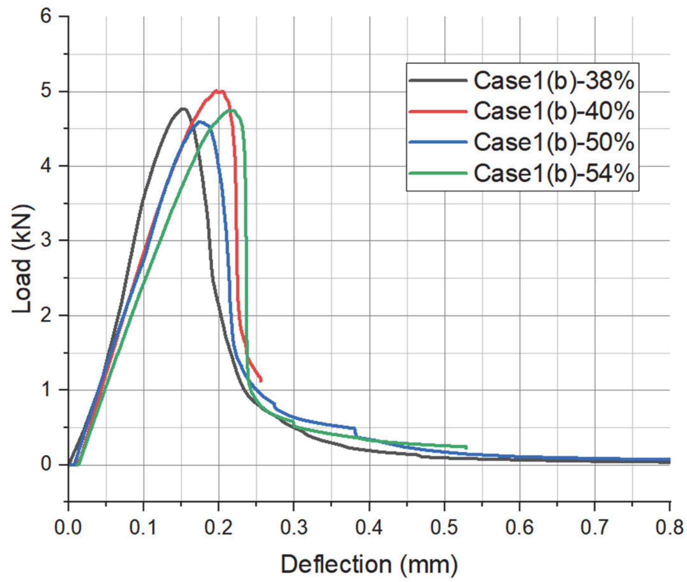

Figure 9: Case1(b) Load-Deflection comparison.

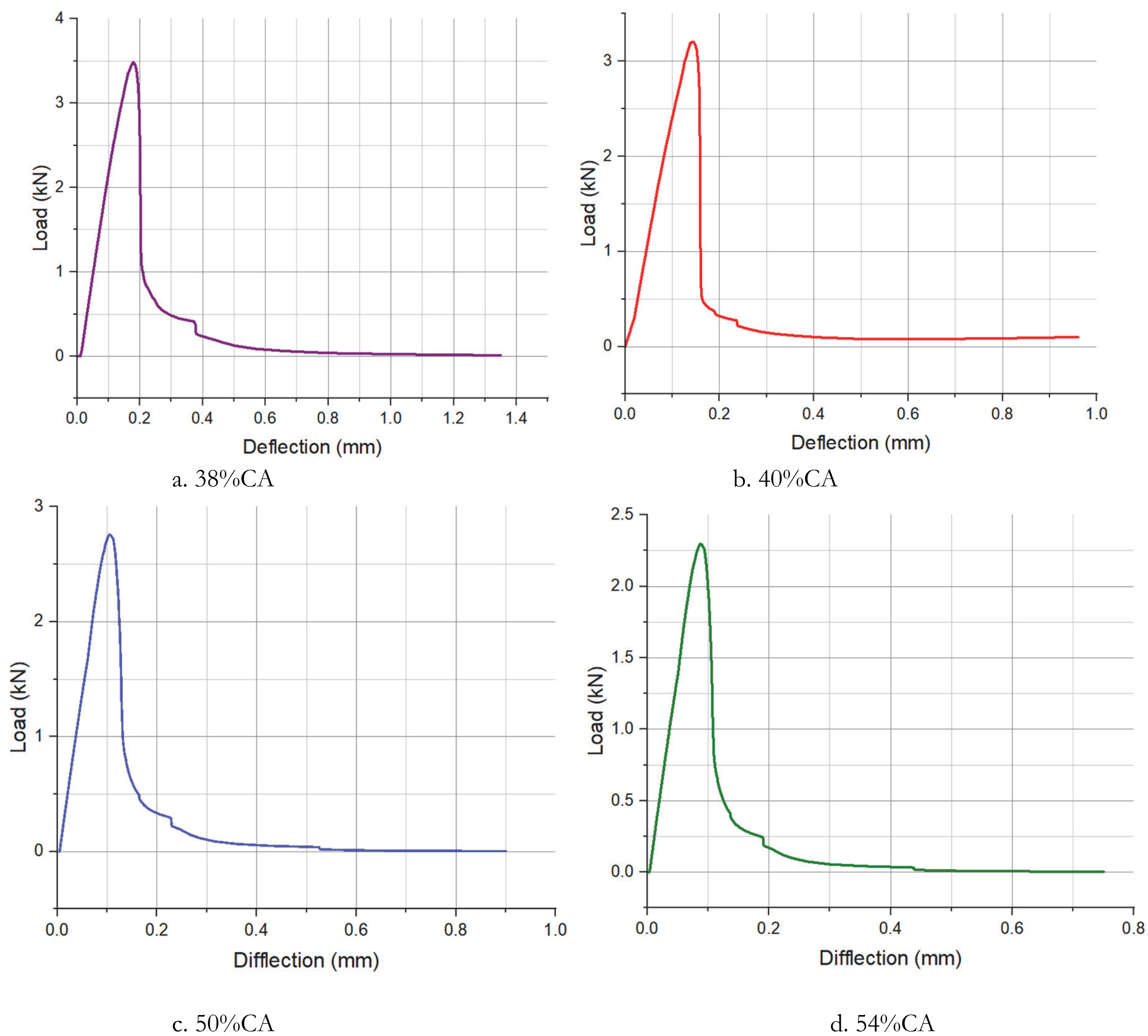

Figure 10: Case2(a) Load -Deflection curve for CA of mean size 12.5mm with ITZ.

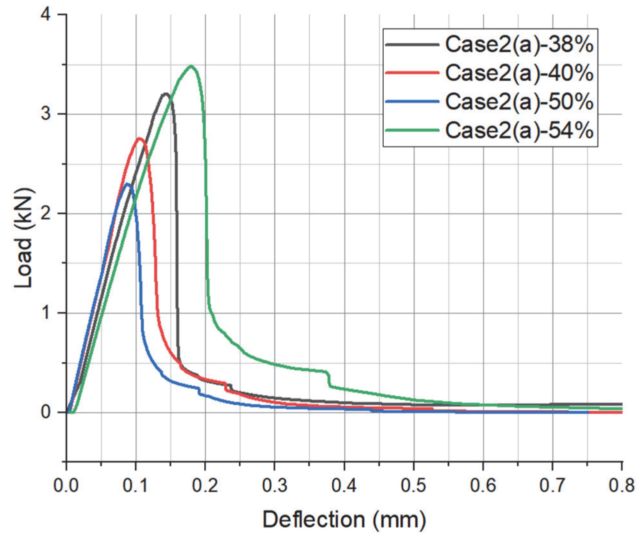

Figure 11: Case2(a) Load-Deflection comparison.

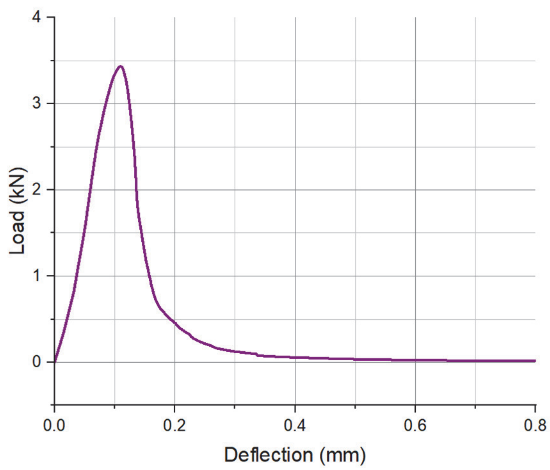

a. 38%CA

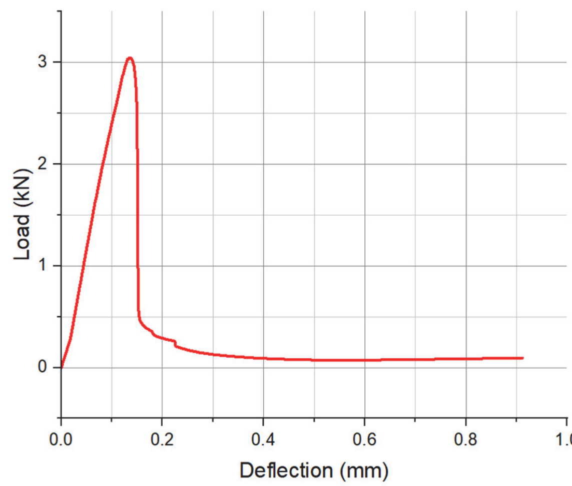

b. 40%CA

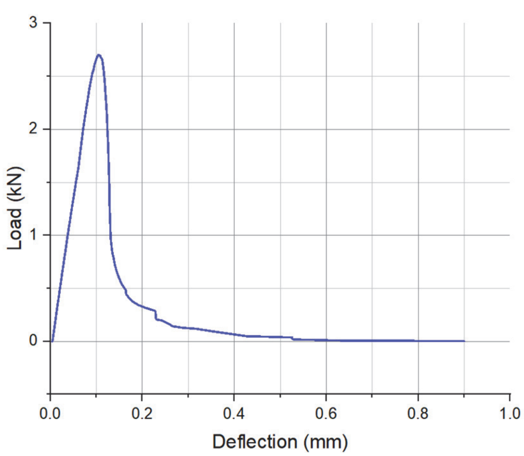

c. 50%CA

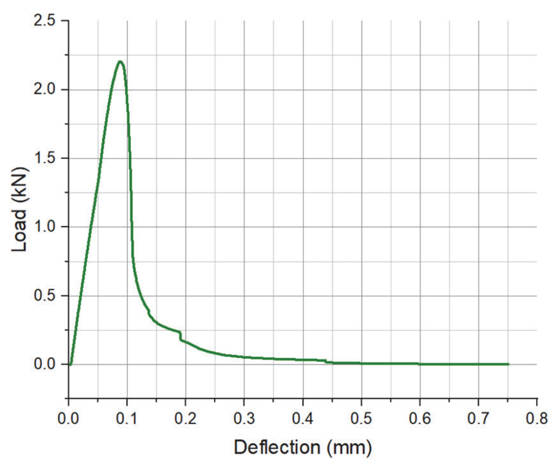

d. 54%CA

Figure 12: Case2(b) Load -Deflection curve for CA of mean size between 4.75mm to 20mm with ITZ.

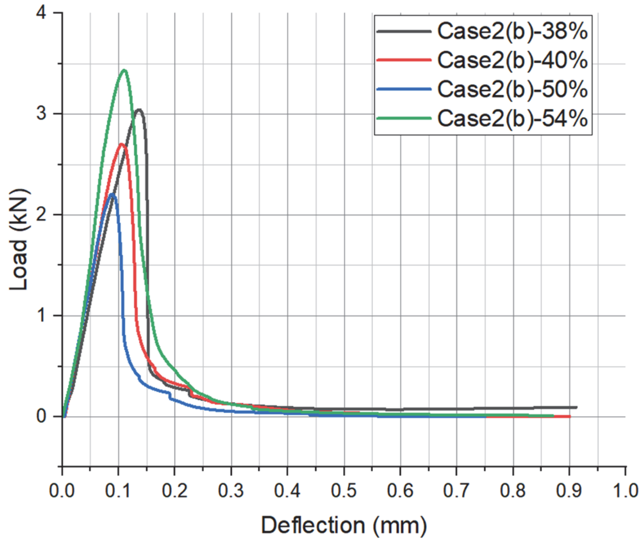

Figure 13: Case2(b) Load-Deflection comparison.

Fraction of CA		Mean size of Aggregate12.5mm (a)				Aggregate size between 4.75mm to 20mm (b)			
		54%	50%	40%	38%	54%	50%	40%	38%
S-B1	Model-1	0.37	0.36	0.21	0.19	0.20	0.18	0.22	0.16
	Model-2	0.25	0.30	0.19	0.18	0.22	0.20	0.18	0.14
	Model-3	0.22	0.21	0.22	0.21	0.19	0.19	0.16	0.13
Mean (μ)		0.28	0.29	0.21	0.19	0.20	0.19	0.28	0.29
Standard Deviation(σ)		0.06	0.06	0.01	0.01	0.01	0.01	0.06	0.06
μ±3σ(99.7%)		0.47	0.47	0.24	0.23	0.24	0.21	0.47	0.47
		0.09	0.11	0.17	0.16	0.17	0.17	0.09	0.11

Table 5: Displacement (mm) at maximum load for Case1(a) and (b).

Fraction of CA		Mean size of Aggregate12.5mm (a)				Aggregate size between 4.75mm to 20mm (b)			
		54%	50%	40%	38%	54%	50%	40%	38%
S-B1	Model-1	0.09	0.11	0.14	0.17	0.09	0.11	0.14	0.11
	Model-2	0.11	0.13	0.16	0.15	0.10	0.13	0.13	0.12
	Model-3	0.15	0.12	0.15	0.14	0.12	0.13	0.12	0.10
Mean (μ)		0.50	0.66	0.68	0.78	0.53	0.70	0.77	0.88
Standard Deviation(σ)		0.50	0.66	0.68	0.78	0.53	0.70	0.77	0.88
μ±3σ(99.7%)		0.12	0.12	0.15	0.15	0.10	0.12	0.12	0.12
		0.02	0.01	0.01	0.01	0.01	0.01	0.02	0.01

Table 6: Displacement (mm) at maximum load for Case 2 (a) and (b).

Fraction of CA		Mean size of Aggregate12.5mm (a)				Aggregate size between 4.75mm to 20mm (b)			
		54%	50%	40%	38%	54%	50%	40%	38%
S-B1	Model-1	296.39	288.12	245.57	245.57	275.12	253.55	256.21	255.91
	Model-2	290.23	270.15	230.22	200.27	260.22	270.20	220.61	230.22
	Model-3	288.12	250.22	225.14	227.5	240.15	220.15	240.12	242.1
Mean (μ)		291.58	269.50	233.64	224.45	258.50	247.97	238.98	242.74
Standard Deviation(σ)		3.51	15.48	8.68	18.62	14.33	20.81	14.56	10.50
μ±3σ(99.7%)		302.11	315.94	259.70	280.30	301.48	310.40	282.65	274.24
		281.05	223.06	207.59	168.59	215.51	185.53	195.31	211.25

Table 7: Fracture Energy, G_F (N/m) for Case1(a) and (b) [4].

Fraction of CA		Mean size of Aggregate12.5mm (a)				Aggregate size between 4.75mm to 20mm (b)			
		54%	50%	40%	38%	54%	50%	40%	38%
S-B1	Model-1	127.08	144.22	207.45	207.45	127.08	134.17	153.38	153.68
	Model-2	120.22	145.6	201.30	166.5	129.34	140.10	144.35	140.22
	Model-3	128.30	140.22	188.70	200.2	145.32	130.11	148.32	120.15
Mean (μ)		125.20	143.35	199.15	191.38	133.91	134.79	148.68	138.02
Standard Deviation(σ)		3.56	2.28	7.80	17.84	8.12	4.10	3.70	13.78
μ±3σ(99.7%)		135.87	150.19	222.56	244.91	158.27	147.10	159.77	179.35
		114.53	136.50	175.74	137.86	109.56	122.49	137.60	96.69

Table 8: Fracture Energy, G_F (N/m) for Case2(a) and (b)

Peak load as per Tabs. 3 and 4: Case 1 (a) ranges from 2.8 kN to 4.0 kN, Case 1 (b) ranges from 4 kN to 5.3 kN, Case 2 (a) ranges from 2.5 kN to 3.5 kN, and Case 2 (b) ranges from 2.2 to 3.6 kN.In the case of uniform aggregate size, the peak load for notched beams shows less compared to non-uniform aggregates due to the resistance to fracture caused by the interlocking of aggregates, and the aggregates are also quite hard. Whereas in the case of a model with ITZ, the peak load reduces due to the ITZ zone. The numerical prediction for the maximum load on the S-B1 beam falls within the range of 3.5 to 3.6 kN, which closely aligns with the experimentally observed values ranging from 3.5 to 3.8 kN [22]. Case 2(b) gives a realistic peak load that can be comparable with the experimental data.

Fracture energy (GF) as per Tabs. 7 and 8 Case 1 (a) ranges from 225 to 296 N/m, Case 1 (b) ranges from 220 to 275 N/m, Case 2 (a) ranges from 120 to 207 N/m, and Case 2 (b) ranges from 120 to 145 N/m. In the case of uniform aggregate size, the peak load for notched beams shows more GF compared to non-uniform aggregates due to the resistance to fracture created by the interlocking of aggregates. Whereas in the ITZ model, GF reduces due to the ITZ zone. The numerical prediction for the GF on the S-B1 beam falls within the range of 120 to 154 kN, which closely aligns with the experimentally observed values ranging from 146N/m to 154N/m kN [22]. Case 2(b) gives realistic GF, which can be comparable with the experimental data.

Post-peak softening slope as per Tabs. 9 and 10 is shallow for Case 2(b). When θ is smaller and softens more and more, ductility increases more and more. From Tabs. 8, 9, and 10, it is observed that the value of tan θ is less for Case 2(b). The inclusion of ITZ leads to a flat slope, which indicates that ITZ enhances the ductility of concrete.

	Mean size of Aggregate12.5mm (a)				Aggregate size between 4.75mm to 20mm (b)			
Fraction of CA	54%	50%	40%	38%	54%	50%	40%	38%
Softening Slope	190	182	177	86	181	180	150	68

Table 9: Load vs Deflection-Slope of the curve (tan θ) for Case1(a) and (b).

Fraction of CA	Mean size of Aggregate12.5mm (a)				Aggregate size between 4.75mm to 20mm (b)			
	54%	50%	40%	38%	54%	50%	40%	38%
Softening Slope	160	150	143	93	85	78	70	60

Table 10: Load vs Deflection-Slope of the curve (tan θ) for Case2(a) and (b).

38% of CA	Case1(a)	Case1(b)	Case2(a)	Case2(b)
Softening Slope	167	33	77	27.76

Table 11: Load vs Deflection-Slope of the curve (tan θ) for all Cases of 38%CA.

The Load-CMOD (Crack Mouth Opening Displacement) plots have also been obtained, revealing a triphasic pattern of behavior. Initially, during the first stage, deflection shows a linear increase alongside incremental loading. At this point, crack initiation transpires without immediate propagation. Subsequently, in the second stage, nonlinear tendencies emerge, causing the plot's slope to decline until it reaches its zenith. Within this phase, the formation of a fracture zone becomes evident due to the existence of microcracks, and crack propagation occurs at a subdued pace. The third stage is recognized as the strain softening zone, characterized by accelerated crack propagation owing to heightened stress concentration. This concentration of stress is particularly pronounced in the narrow region between the notch tip and the loading point. The stress concentration is higher as the load-carrying capacity decreases, leading to the failure of the specimen. From Tab.11, it is observed that the value of tan θ is less for Case 2(b), indicating the ductile behavior of concrete with respect to CMOD under load. Fig. 14 shows the comparative study of the inclusion of 38% CA for all cases which reveals similar results as that of Load displacement curves.

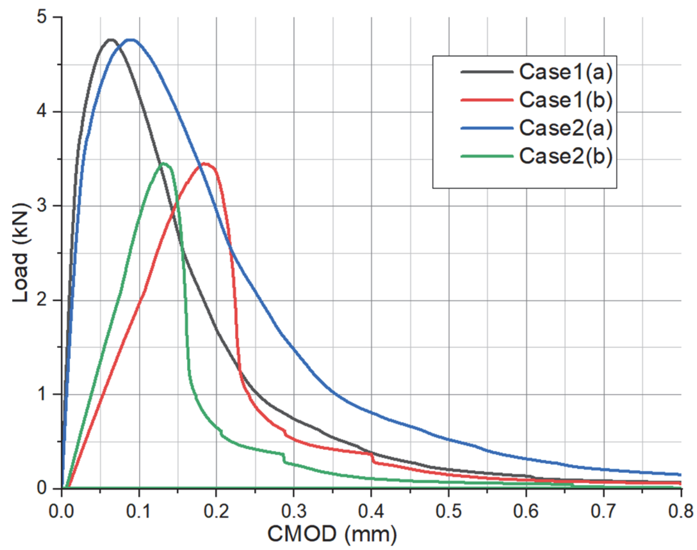

Figure 14: Load-CMOD comparison for CA of 38% (All cases)

Conclusions

In the case of a model without ITZ, the peak load observed is greater than the experimental value; this could be due to the resistance offered by the aggregate well before compared to when the crack was hard to pass through the ITZ. When the interface is introduced, whose tensile strength is lower than that of the matrix, cracks will progress through the ITZ but pass around the aggregate. In that case, the peak load from the simulation closely matches the experimental result.

Particularly, post-peak softening behavior, which is indicated by the gradual decrease in slope, indicates that concrete behavior is relatively ductile in nature. It shows an improvement in ductility due to the introduction of ITZ, which represents a realistic concrete model. The softening slope is the most precious parameter, which tells us what type of mix can give a more softening effect, and it is better to have a shallow softening slope.

The Extended Finite Element Method (XFEM), along with Cohesive Element, effectively used for multiscale modeling of concrete to assess fracture behavior, appears to be more appropriate. Modeling the cohesive zone model along with the effect of the texture of aggregates on the simulation of fractures in concrete beams would be the focus of a future study.

References

[1] Barenblatt, G.. (1959). The formation of equilibrium cracks during brittle fracture. General ideas and hypotheses. Axially-symmetric cracks, J. Appl. Math. Mech., 23(3), pp. 622–36, DOI: 10.1016/0021-8928(59)90157-1.

[2] Hillerborg, A., Modéer, M., Petersson, P.E. (1976). Analysis of crack formation and crack growth in concrete by means of fracture mechanics and finite elements, Cem. Concr. Res., 6(6), pp. 773–781, DOI: 10.1016/0008-8846(76)90007-7.

[3] Bažant, Z.P., Oh, B.H. (1983). Crack band theory for fracture of concrete, Matériaux Constr., 16(3), pp. 155–177, DOI: 10.1007/BF02486267.

[4] Rilem. FMC-50(1985). Determination of the fracture energy of mortar and concrete by means of three-point bend tests on notched beams, Mater. Struct., 18, pp. 287-290, DOI: 10.1007/BF02472918.

[5] Ananthan, H., Raghuprasad, B.K., Sundara, K.T., Iyengar, R. (1990). Influence of strain softening on the fracture of plain concrete beams, Int. J. Fract., 45(3), pp. 195–219, DOI: 10.1007/BF00693349.

[6] Sundara Raja Iyengar, K.T., Raghuprasad, B.K., Nagaraj, T.S., Patel, B. (1997). Determination of load-deflection curve of plain concrete beams from the softening beam model, J. Struct. Eng., 24(1), pp. 11–15.

[7] Elices, M., Guinea, G. V., Gómez, J., Planas, J. (2001). The cohesive zone model: Advantages, limitations and challenges, Eng. Fract. Mech., 69(2), pp. 137–163, DOI: 10.1016/S0013-7944(01)00083-2.
[8] Elsharief, A., Cohen, M.D., Olek, J. (2003). Influence of aggregate size, water cement ratio and age on the microstructure of the interfacial transition zone, Cem. Concr. Res., 33(11), pp. 1837–49, DOI: 10.1016/S0008-8846(03)00205-9.
[9] Chen, B., Liu, J. (2004). Effect of aggregate on the fracture behavior of high strength concrete, Constr. Build. Mater., 18(8), pp. 585–590, DOI: 10.1016/j.conbuildmat.2004.04.013.
[10] Akçaoğlu, T., Tokyay, M., Çelik, T. (2004). Effect of coarse aggregate size and matrix quality on ITZ and failure behavior of concrete under uniaxial compression, Cem. Concr. Compos., 26(6), pp. 633–638, DOI: 10.1016/S0958-9465(03)00092-1.
[11] Song, S.H., Paulino, G.H., Buttlar, W.G. (2006). A bilinear cohesive zone model tailored for fracture of asphalt concrete considering viscoelastic bulk material, Eng. Fract. Mech., 73(18), pp. 2829–2848, DOI: 10.1016/j.engfracmech.2006.04.030.
[12] Oliver, J., Huespe, A.E., Sánchez, P.J. (2006). A comparative study on finite elements for capturing strong discontinuities: E-FEM vs X-FEM, Comput. Methods Appl. Mech. Eng., 195(37–40), pp. 4732–4752, DOI: 10.1016/j.cma.2005.09.020.
[13] Kozicki, J., Tejchman, J. (2007).Effect of aggregate structure on fracture process in concrete using 2D lattice model. Archives of Mechanics, 59, pp. 365–384.
[14] Sagar, R.V., Prasad, B.K.R., Gopalakrishnan, A.R. (2008). Size-independent specific fracture energy of high strength concrete beams using hybrid method, Indian Concr. J., 82(11), pp. 30–42.
[15] Danielson, K.T., Akers, S.A., O'Daniel, J.L., Adley, M.D., Garner, S.B. (2008). Large-Scale Parallel Computation Methodologies for Highly Nonlinear Concrete and Soil Applications, J. Comput. Civ. Eng., 22(2), pp. 140–146, DOI: 10.1061/(asce)0887-3801(2008)22:2(140).
[16] Akcay, B., Agar-Ozbek, A.S., Bayramov, F., Atahan, H.N., Sengul, C., Tasdemir, M.A. (2012). Interpretation of aggregate volume fraction effects on fracture behavior of concrete, Constr. Build. Mater., 28(1), pp. 437–443, DOI: 10.1016/j.conbuildmat.2011.08.080.
[17] Huang, J., Chen, M., Sun, J. (2014). Mesoscopic characterization and modeling of microcracking in cementitious materials by the extended finite element method, Theor. Appl. Mech. Lett., 4(4), pp. 041001, DOI: 10.1063/2.1404101.
[18] Michels, J., Zile, E., Czaderski, C., Motavalli, M. (2014). Debonding failure mechanisms in prestressed CFRP/epoxy/concrete connections, Eng. Fract. Mech., 132, pp. 16–37, DOI: 10.1016/j.engfracmech.2014.10.012.
[19] Huang, Y., Yang, Z., Ren, W., Liu, G., Zhang, C. (2015). 3D meso-scale fracture modelling and validation of concrete based on in-situ X-ray Computed Tomography images using damage plasticity model, Int. J. Solids Struct., 67–68, pp. 340–352, DOI: 10.1016/j.ijsolstr.2015.05.002.
[20] Wang, X.F., Yang, Z.J., Yates, J.R., Jivkov, A.P., Zhang, C. (2015). Monte Carlo simulations of mesoscale fracture modelling of concrete with random aggregates and pores, Constr. Build. Mater., 75, pp. 35–45, DOI: 10.1016/j.conbuildmat.2014.09.069.
[21] Abdel Wahab, M.M. (2015).Simulating mode I fatigue crack propagation in adhesively-bonded composite joints. Fatigue and Fracture of Adhesively-Bonded Composite Joints, pp. 323–344.
[22] Trivedi, N., Singh, R.K., Chattopadhyay, J. (2015). A comparative study on three approaches to investigate the size independent fracture energy of concrete, Eng. Fract. Mech., 138, pp. 49–62, DOI: 10.1016/j.engfracmech.2015.03.021.
[23] Hussein, H.H., Walsh, K.K., Sargand, S.M., Steinberg, E.P. (2016). Interfacial Properties of Ultrahigh-Performance Concrete and High-Strength Concrete Bridge Connections, J. Mater. Civ. Eng., 28(5), DOI: 10.1061/(asce)mt.1943-5533.0001456.
[24] Trawiński, W., Bobiński, J., Tejchman, J. (2016). Two-dimensional simulations of concrete fracture at aggregate level with cohesive elements based on X-ray μCT images, Eng. Fract. Mech., 168, pp. 204–226, DOI: 10.1016/j.engfracmech.2016.09.012.
[25] Hao, Y., Hao, H. (2016). Finite element modelling of mesoscale concrete material in dynamic splitting test, Adv. Struct. Eng., 19(6), pp. 1027–1039, DOI: 10.1177/1369433216630828.
[26] Zhou, R., Song, Z., Lu, Y. (2017). 3D mesoscale finite element modelling of concrete, Comput. Struct., 192, pp. 96–113, DOI: 10.1016/j.compstruc.2017.07.009.
[27] Zhang, Z., Song, X., Liu, Y., Wu, D., Song, C. (2017). Three-dimensional mesoscale modelling of concrete composites by using random walking algorithm, Compos. Sci. Technol., 149, pp. 235–245, DOI: 10.1016/j.compscitech.2017.06.015.
[28] Wang, J., Jivkov, A.P., Engelberg, D.L., Li, Q.M. (2019).Parametric Study of Cohesive ITZ in Meso-scale Concrete Model. Procedia Structural Integrity, 23, pp. 167–72.

[29] Wu, Z., Cui, W., Fan, L., Liu, Q. (2019). Mesomechanism of the dynamic tensile fracture and fragmentation behaviour of concrete with heterogeneous mesostructure, Constr. Build. Mater., 217, pp. 573–591, DOI: 10.1016/j.conbuildmat.2019.05.094.
[30] Chen, H., Xu, B., Wang, J., Nie, X., Mo, Y.L. (2020). XFEM-based multiscale simulation on monotonic and hysteretic behavior of reinforced-concrete columns, Appl. Sci., 10(21), pp. 1–21, DOI: 10.3390/app10217899.
[31] Rhardane, A., Alam, S.Y., Grondin, F. (2020). Microscopically informed upscale approach of modelling damage in mortar by considering matrix-to-grain interface and grain micro-fracture characteristics, Theor. Appl. Fract. Mech., 109, DOI: 10.1016/j.tafmec.2020.102725.
[32] Fidi, F., Muin, R.B., Patty, A.H. (2020).The effect of aggregate gradation on concrete fracture energy using the work of fracture method. IOP Conference Series: Materials Science and Engineering, 830, DOI:10.1088/1757-899X/830/2/022061.
[33] Maleki, M., Rasoolan, I., Khajehdezfuly, A., Jivkov, A.P. (2020). On the effect of ITZ thickness in meso-scale models of concrete, Constr. Build. Mater., 258, DOI: 10.1016/j.conbuildmat.2020.119639.
[34] Holla, V., Vu, G., Timothy, J.J., Diewald, F., Gehlen, C., Meschke, G. (2021). Computational generation of virtual concrete mesostructures, Materials (Basel)., 14(14), DOI: 10.3390/ma14143782.
[35] Zhou, R., Lu, Y., Wang, L.G., Chen, H.M. (2021). Mesoscale modelling of size effect on the evolution of fracture process zone in concrete, Eng. Fract. Mech., 245, DOI: 10.1016/j.engfracmech.2021.107559.
[36] Ying, J., Guo, J. (2021). Fracture behaviour of real coarse aggregate distributed concrete under uniaxial compressive load based on cohesive zone model, Materials (Basel), 14(15), DOI: 10.3390/ma14154314.
[37] Talaat, A., Emad, A., Tarek, A., Masbouba, M., Essam, A., Kohail, M. (2021). Factors affecting the results of concrete compression testing: A review, Ain Shams Eng. J.,12(1), pp. 205–221, DOI: 10.1016/j.asej.2020.07.015.
[38] Pei, X., Huang, X., Li, H., Cao, Z., Yang, Z., Hao, D., Min, K., Li, W., Liu, C., Wang, S., Wu, K. (2023). Numerical Simulation of Fatigue Life of Rubber Concrete on the Mesoscale, Polymers (Basel)., 15(9), DOI: 10.3390/polym15092048.
[39] Ji, H., Yang, X., Luo, Z., Bai, F. (2023). Tensile Fracture Property of Concrete Affected by Interfacial Transition Zone, Int. J. Concr. Struct. Mater., 17(1), DOI: 10.1186/s40069-022-00564-2.
[40] Luu, X.B., Kim, S.K. (2023). Finite Element Modeling of Interface Behavior between Normal Concrete and Ultra-High Performance Fiber-Reinforced Concrete, Buildings, 13(4), DOI: 10.3390/buildings13040950.
[41] Suchan, T., Najafi Koopas, R., Rauter, N., Welker, K. (2023). Tracking of fracture-state displacement data generated by cohesive zone modeling using shape optimization, Pamm, 22(1), DOI: 10.1002/pamm.202200284.